Proceedings RootS25
3rd International Workshop on Soil-Vegetation-Atmosphere Interaction
Boldrin D, Cecconi M, Cotecchia F, Leung A, Pedone G, Perrini P, Romero E, Tagarelli V, Zdravković L (eds)
ISSN: 3107-300X

doi: doi.org/10.53243/RootS2025-62

Anisotropic behaviour of rooted soils: constitutive modelling

Ali Akbar Karimzadeh [1], Anthony Kwan Leung[2], Zhiwei Gao[3], Raul Fuentes[1]

[1]*Chair of Geotechnical Engineering and Institute of Geo-mechanics and Underground Technology, RWTH Aachen University, Aachen, Germany*

[2]*State Key Laboratory of Climate Resilience for Coastal Cities, Department of Civil and Environmental Engineering, Hong Kong University of Science and Technology, Hong Kong SAR, China*

[3] *Glasgow Computational Engineering Centre (GCEC), James Watt School of Engineering, University of Glasgow, Glasgow, UK.*

ABSTRACT: Plant roots enhance soil stability, offering sustainable solutions for mitigating slope failure, erosion, and liquefaction. Experimental studies on rooted soils have revealed anisotropic and stress-dependent reinforcement effects. However, the theoretical understanding of this anisotropic behaviour remains limited. To interpret these behaviours, an anisotropic constitutive model was developed within the anisotropic critical state theory framework, incorporating two independent fabric tensors to represent the evolving structures of soil and roots. New anisotropic variables (A_B, A_R) and a root network evolution rule were introduced to capture the progressive mobilisation of root tensile strength as roots reoriented toward the direction perpendicular to the major principal stress. The model successfully reproduced key features of rooted soil behaviour under monotonic loadings, providing a unified framework for predicting the complex mechanical response of rooted soils.

Keywords: Vegetated soil; Anisotropy; Constitutive model; Root tensile mobilisation; Root orientation evolution

1 INTRODUCTION

Plants stabilise shallow soils by enhancing the shear strength through two primary mechanisms: (i) mobilisation of root tensile strength via stress transfer along the soil–root interface, and (ii) increase in matric suction due to transpiration (Ng et al., 2019; Karimzadeh et al., 2024a). Becasue root system architecture varies amongst species and the loading direction relative to root orientation differs under various stress paths (Figure 1), recent studies have shown that the mechanical behaviour of rooted soils is anisotropic and stress-dependent under monotonic (Karimzadeh et al., 2021, 2024a, 2024b) and cyclic (Karimzadeh et al., 2021, 2022) loading conditions. Consequently, the behaviour of rooted soils—in terms of failure criterion, maximum shear modulus, and constitutive model—should be considered anisotropic in generalised loading conditions.

In the literature, two main approaches have been used to construct constitutive models of rooted soils. The first treats rooted soil as a continuum and incorporates root effects within elastoplastic frameworks, such as modified Cam-Clay or state-dependent models that account for root-induced hardening through mechanisms like pore occupancy and bonding (Switala & Wu, 2018). The second approach models soil and roots as separate interacting phases, each governed by its constitutive law, providing detailed insights into their stress–strain behaviour but requiring complex parameterisation due to root heterogeneity (Muir Wood et al, 2016; Meijer et al., 2023). Although effective under limited stress paths, both approaches are unable to capture the anisotropic behaviour of rooted soils under general 3D loading conditions. Anisotropy of rooted soil arises from the combined effects of inherent fabric and root network as well as induced anisotropy during shearing, where root orientation evolves and progressively mobilises tensile and interfacial strength (Karimzadeh et al., 2021, 2024a; Meijer et al., 2023). However, no theoretical framework exists to describe the coupled evolution of soil and root fabric within an anisotropic critical-state theory (ACST) context.

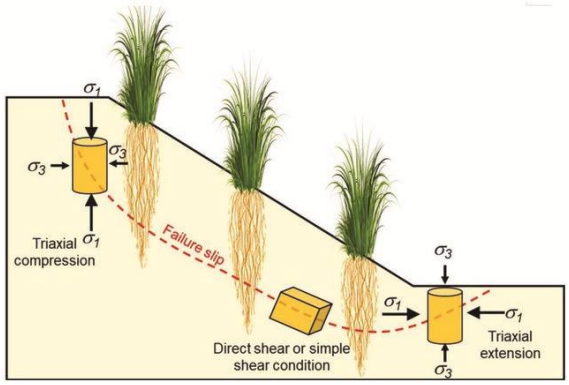

Figure 1. Rotation of principal stresses along the failure surface relative to root orientation (Karimzadeh et al. 2021)

In this paper, the anisotropic behaviour of rooted soil is investigated through constitutive modelling, building upon the recent study by Karimzadeh et al. (2025). The

model employs two independent fabric tensors to represent the soil fabric and root network, enabling the quantification of their combined influence on soil anisotropy under general 3D loading conditions. A new evolution law is introduced to capture the reorientation of the root network during shearing and its contribution to stress transfer along the soil–root interface. Three additional parameters are incorporated to represent the mechanical effects of roots, extending the applicability of conventional models for bare soils. The proposed model is validated against experimental data covering different stress paths and overconsolidation ratios under drained and undrained conditions, demonstrating its capability to reproduce the key anisotropic features of rooted soils and its potential application in the analysis and design of vegetated slopes and infrastructures.

2 CONSITUTIVE MODEL

The anisotropic constitutive model for rooted soils was established based on the anisotropic critical state framework proposed by Li and Dafalias (2002, 2012) and the formulation is given in Table 1. All symbols used in Table 1 are defined in the Notation section. It incorporates the coupled effects of (1) fabric anisotropy and its evolution; (2) the root network (Equation 13); and (3) root orientation evolution on the mechanical behaviour of rooted soils (Equation 15). A cone-shaped yield surface (Equation 1) and the associated ACST are adopted. Two fabric tensors—one for the bare soil (F_{ij}) and one for the root network (R_{ij}) (Equation 12 & 13) —govern the directional dependence of the mechanical response. Their evolution laws describe how the internal structure of both soil and root networks gradually realigns under deviatoric loading. As plastic deformation progresses, R_{ij} evolves according to the stress path, gradually reorienting perpendicular to the major principal stress direction, where the roots would be exposed to the maximum tensile strain, thus the maximum tensile mobilisation. This reorientation decreases A_R (Equation 17), thereby reducing ζ (Equation 18) and leading to higher plastic modulus K_P and shear resistance (Eqs.19 & 21).

3 MODEL VALIDATION

The proposed model has 18 parameters, grouped into five categories: (1) elasticity (G_0, ν), (2) critical-state (M_c, c, e_Γ, λ_c, ξ), (3) dilatancy (d_0, m), (4) hardening (h_1, h_2, n), and (5) fabric evolution (F_0, R_0, e_A, e_R, k_f, k_r) , with three parameters (R_0, e_R, k_r) describing root effects. Elasticity parameters G_0 and ν are obtained from the maximum shear modulus of bare soil at very small strains (Karimzadeh et al., 2024b), and critical-state parameters are determined from compression and extension tests of bare soil, assuming roots have negligible influence on G_0, M_c, and c (Karimzadeh et al., 2021). The remaining parameters are calibrated by fitting stress–strain, stress path (p'–q), and volumetric strain data for bare and rooted soils, with R_0, e_R, and k_r calibrated to capture the root effects on soil behaviour.

Table 1. Summary of model equations and definitions

Equations	Description	Eq. No.
$f(\boldsymbol{r_{ij}}, H) = \frac{R}{g(\theta)} - H = 0$	Yield function	Eq. 1
$R = \sqrt{\frac{3}{2}\boldsymbol{r_{ij}}\boldsymbol{r_{ij}}}$	Deviatoric stress ratio invariant	Eq. 2
$g(\theta) = \frac{\sqrt{(1+c^2)^2 + 4c(1-c^2)\sin 3\theta} - (1+c^2)}{2(1-c)\sin 3\theta}$	Lode-angle interpolation; $c=M_e/M_c$	Eq. 3
$de^p_{ij} = \langle dL \rangle n_{ij}$	Plastic strain increment	Eq. 4
$d\varepsilon^p_v = \sqrt{\frac{2}{3}}\langle dL \rangle D$	Plastic volumetric strain	Eq. 5
$d\varepsilon^p_{ij} = \langle dL \rangle \left(n_{ij} + \sqrt{\frac{2}{27}} D\delta_{ij} \right) = \langle dL \rangle N_{ij}$	Total plastic strain	Eq. 6
$de^e_{ij} = \frac{ds_{ij}}{2G} = \frac{pdr_{ij}}{2G} + \frac{r_{ij}dp'}{2G}$	Elastic deviatoric strain increment	Eq. 7
$d\varepsilon^e_v = \frac{dp'}{K}$	Elastic volumetric strain increment	Eq. 8
$G = G_0 \frac{(2.97-e)^2}{1+e}\sqrt{p' p_a}$	Elastic shear modulus	Eq. 9
$K = G\frac{2(1+\nu)}{3(1-2\nu)}$	Elastic bulk modulus	Eq. 10
$d\sigma_{ij} = (E_{ijlk} - h(dL)E_{ijmn}N_{mn}\Pi_{kl})\, d\varepsilon_{kl} = \Lambda_{ijkl}\, d\varepsilon_{kl}$	Elastoplastic stress increment	Eq. 11
$F_{ij} = \sqrt{\frac{2}{3}}\begin{bmatrix} F_0 & 0 & 0 \\ 0 & \frac{-F_0}{2} & 0 \\ 0 & 0 & \frac{-F_0}{2} \end{bmatrix}$	Fabric tensor for bare soil	Eq. 12
$\mathcal{R}_{ij} = \sqrt{\frac{2}{3}}\begin{bmatrix} \mathcal{R}_0 & 0 & 0 \\ 0 & -\frac{\mathcal{R}_0}{2} & 0 \\ 0 & 0 & -\frac{\mathcal{R}_0}{2} \end{bmatrix}$	Fabric tensor for root network	Eq. 13
$dF_{ij} = \langle dL \rangle k_f (n_{ij} - F_{ij})$	Soil fabric evolution	Eq. 14
$d\mathcal{R}_{ij} = \langle dL \rangle k_r (-n_{ij} - \mathcal{R}_{ij})$	Root network evolution	Eq. 15
$A_B = F_{ij}n_{ij}$	Fabric anisotropy state variables	Eq. 16
$A_R = \mathcal{R}_{ij}n_{ij}$	State variables for roots	Eq. 17
$\zeta = \psi - e_A(A_B - 1) + e_R(A_R - 1)$	Dilatancy state parameter	Eq. 18
$K_p = \frac{Gh}{R}[M_c g(\theta)\exp(-n\zeta) - R]$	Plastic modulus	Eq. 19
$h = (1 - h_1 e)\exp(h_2 A_B)$	Plastic modulus factor	Eq. 20
$D = \frac{d_0}{M_c g(\theta)}\left(1 + \frac{R}{M_c g(\theta)}\right)[M_c g(\theta)\exp(m\zeta) - R]$	Dilatancy	Eq. 21

The value of R_0 is typically set at 0.7, reflecting the vertical growth of tap roots. Ideally, e_R is calibrated from the critical-state line (CSL) of rooted soils in e–log(p') space; however, as CSL is often reached at large strains (~100%), k_r and e_R can also be calibrated by iteratively adjusting them so that the plastic hardening modulus K_p

(Equation 19) reaches zero at peak shear strength during drained triaxial tests. The calibration requires multiple iterations because the root network evolution depends on k_r and e_R. The F_0 value was obtained by fitting triaxial compression and extension data at p' = 100 kPa. Calibration results showed F_0 = 0.7 for dry-deposited artificial samples and F_0 = −0.1 for moist-compacted cultivated samples, indicating more horizontal particle alignment in the former and near-isotropic fabric in the latter, due to matric suction, resulting in more isotropic fabric and smaller differences between compression and extension paths.

Table 2. Parameters for rooted sand and silty sand samples

Parameter Category	Parameter	Artificial Rooted Sand	Cultivated Rooted Silty Sand
Elasticity	G_0	125	125
	ν	0.15	0.15
Critical state	M_c	1.25	1.40
	c	0.75	0.9
	e_Γ	0.934	0.935
	λ_c	0.019	0.086
	ξ	0.7	N.A
Dilatancy	d_0	0.25	0.5
	m	1.5	5
Hardening	h_1	1	0.9
	h_2	0.9	0.95
	n	1	0.5
Fabric evolution	F_0	0.7	-0.1
	R_0	0.67	0.7
	e_A	0.085	0.085
	e_R	0.090	0.040
	k_f	3	10
	k_r	5	1

**Noted: all parameters are dimensionless.*

Figure 2(a) compares the model predictions with the data of undrained triaxial compression and extension tests on bare Toyura sand at a void ratio of 0.67 at different confinements. Note that in Figures 2 and 3, '*B*' refers to bare soil, and '*R*' refers to rooted soil. The soils subjected to compression path showed pronounced strain-hardening, and those subjected to extension path exhibited strain-hardening, followed by transitional strain-softening or quasi-steady behaviour. Stress paths revealed more contractive behaviour in extension than compression, reflecting fabric anisotropy. Figure 2(b) presents the model predictions for rooted sand. In compression, roots had little effect on the soil strength due to a high A_R, indicating minimal mobilisation of root strength and negligible influence on dilatancy. In extension, the rooted soil displayed a higher shear strength and more dilative response than the bare soil, as A_R approached its critical value (i.e. A_R=-*1*), making the behaviour to switch from strain-softening to strain-hardening.

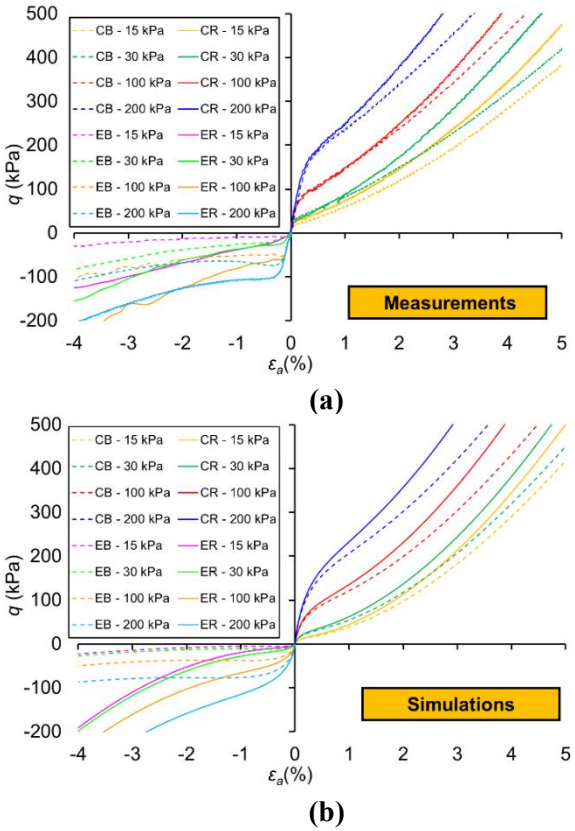

Figure 2. Comparison of bare and artificially rooted sandy soil: (a) experimental results and (b) simulation outcomes

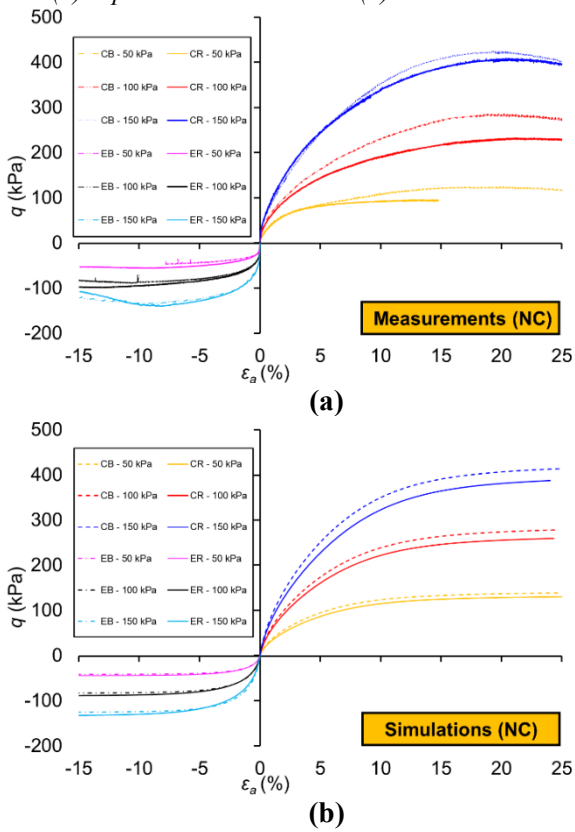

Figure 3. Comparison of bare and normal NC rooted soil: (a) experimental results and (b) simulation outcomes

Figures 3 (a) and (b) compare model predictions with test data for normal consolidation silty sand soil with and without cultivating vetiver roots, respectively. In compression, the rooted soils show lower peak shear

strength than the bare soils due to higher void ratios, reduced compressibility from root resistance, and limited mobilisation of root tensile strength at peak stress. In contrast, in extension, root tensile strength is substantially mobilised as roots align with the minor principal stress, resulting in higher peak shear strength of the rooted soils. The model effectively captures the influence of soil anisotropy and root networks on soil behaviour by incorporating A_R into the dilatancy state parameter and plastic modulus

4 CONCLUSIONS

An anisotropic multiaxial constitutive model for rooted soils has been presented based on Karimzadeh et al. (2025). The model was developed within the anisotropic critical state theory framework and successfully captures the coupled anisotropic behaviour arising from both the soil fabric and the root network. By introducing two anisotropic variables, A_B and A_R, expressed as joint invariants of the loading direction, soil fabric, and root network tensors, the model simulates the evolution of the soil–root structure during plastic deformation. The proposed root network evolution rule effectively reproduces the progressive mobilisation of root tensile strength, controlling changes in hardening and dilatancy. Validation against experimental data under various drainage conditions and stress paths confirms the model's ability to predict key mechanical responses of bare and rooted soils. Whilst the model provides strong agreement for sand and normally consolidated silty sand, refinements such as implementing a bounding surface with a cap could further improve predictions for overconsolidated soils.

5 ACKNOWLEDGEMENTS

The first two authors acknowledge the funding provided by the Hong Kong Research Grant Councils (16202422, N_HKUST603/22, 16206623) and the State Key Laboratory of Climate Resilience for Coastal Cities (ITSC-SKLCRCC26EG01).

6 NOTATIONS

A_B	Fabric anisotropic variables for soil fabric
A_R	Anisotropic variables for root network
D	Dilatancy equation
d_0	Model parameter
dL	Loading index
e	Void ratio
e_A, e_R and e_F,	Model parameters
e_{ij}^e and e_{ij}^p	Elastic and plastic deviatoric strain
F_0	Degree of soil fabric anisotropy
F_{ij}	Deviatoric soil fabric tensor
f	Yield function
G	Elastic shear modulus
G_0	Model parameter
$g(\theta)$	Interpolation function for stress ratio
h_1 and h_2	Model parameters
K	Elastic bulk modulus
M_c, M_e	Critical-state stress ratio in triaxial compression and triaxial extension
m	Model parameter
p	Mean stress
p_a	Atmospheric pressure
R	Stress ratio
RVR	Root volume ratio
R_0	Degree of root network anisotropy
$\mathcal{R}_{ij}$	Deviatoric root network tensor
r_{ij}	Stress ratio tensor
s_{ij}	Deviatoric stress tensor
δ_{ij}	Kronecker delta
ζ	Dilatancy state parameter
ε_{ij}	Total strain tensor
θ	Lode angle of the stress tensor
λ_c	Model parameter
ν	Poisson's ratio
ξ	Model parameter
σ_{ij}	Stress tensor
ψ	State parameter for bare soil

7 REFERENCES

Karimzadeh, A.A., Leung, A.K., Hosseinpour, S., Wu, Z., Fardad Amini, P. 2021. Monotonic and cyclic behaviour of root-reinforced sand, *Can. Geotech. J.* **58**, 1915–1927.

Karimzadeh, A.A., Leung, A.K. Fardad Amini, P. 2022. Energy-based assessment of liquefaction resistance of rooted soil, *J. Geotech. Geoenviron. Eng.* **148**, 1–5.

Karimzadeh, A.A., Leung, A.K., Gao, Z. 2024a. Shear strength anisotropy of rooted soils, *Géotechnique* **74**, 1033–1046.

Karimzadeh, A.A., Leung, A.K., Gao, Z. 2024b. Maximum shear modulus anisotropy of rooted soils, *Géotechnique* (in press).

Karimzadeh, A.A., Leung, A.K., Gao, Z. 2025. Anisotropic constitutive modelling of rooted soils, *Géotechnique* (in press).

Li, X.S., Dafalias, Y.F. 2002. Constitutive modeling of inherently anisotropic sand behavior, *J. Geotech. Geoenviron. Eng.* **128**, 868–880.

Li, X.S., Dafalias, Y.F. 2012. Anisotropic critical state theory: Role of fabric, *J. Eng. Mech.* **138**, 263–275.

Meijer, G.J., Muir Wood, D., Knappett, J.A., Bengough, A.G., Liang, T. 2023. Root reinforcement: continuum framework for constitutive modelling, *Géotechnique* **73**, 600–613.

Muir Wood, D., Diambra, A., Ibraim, E. 2016. Fibres and soils: a route towards modelling of root–soil systems, *Soils Found.* **56**, 765–778.

Ng, C., Leung, A., Ni, J. 2019. *Plant-soil slope interaction,* CRC Press, Boca Raton, FL.

Świtała, B.M., Wu, W. 2018. Numerical modelling of rainfall-induced instability of vegetated slopes, *Géotechnique* **68**, 481–491.